ACS APPLIED MATERIALS & INTERFACES

Research Article

www.acsami.org

Low-Work-Function, ITO-Free Transparent Cathodes for Inverted Polymer Solar Cells

Zhichao Xue,[†,‡] Xingyuan Liu,[*,†] Ying Lv,[†] Nan Zhang,[†] and Xiaoyang Guo[*,†]

[†]State Key Laboratory of Luminescence and Applications, Changchun Institute of Optics, Fine Mechanics and Physics, Chinese Academy of Sciences, Changchun 130033, China

[‡]University of Chinese Academy of Sciences, Beijing 100049, China

Supporting Information

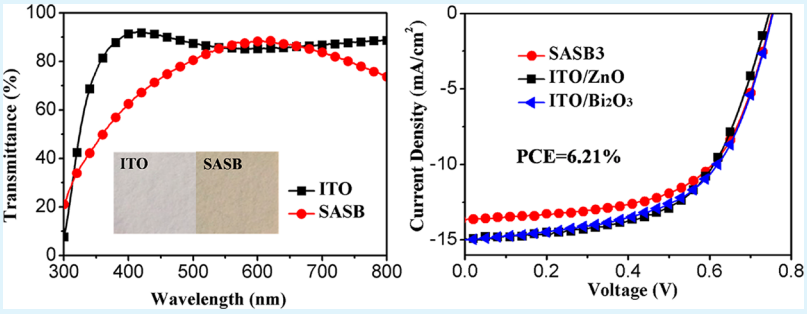

ABSTRACT: A low-work-function, indium tin oxide (ITO)-free transparent cathode having a tin oxide (SnO_X)/Ag/SnO_X/bismuth oxide (Bi_2O_3) (SASB) structure is developed without using annealing treatment. This represents the first time that Bi_2O_3 has been introduced to lower the work function of transparent electrodes. The SASB transparent cathode exhibits excellent photoelectric properties with a maximum transmittance of ~88%, a low sheet resistance of ~9.0 $\Omega \cdot sq^{-1}$, and a suitable work function of 4.22 eV that matches the lowest unoccupied molecular orbital level of the acceptor for exacting electrons efficiently. The power conversion efficiency of the polymer solar cell with the SASB electrode is 6.21%, which is comparable to that of ITO-based devices. The results indicate that SASB is a good alternative to ITO as transparent cathodes in optoelectronic devices.

KEYWORDS: *transparent cathode, ITO-free, work function, polymer solar cell, bismuth oxide*

INTRODUCTION

Polymer solar cells (PSCs) attract considerable interest as renewable energy sources that exhibit unique properties, such as their lightweight, low cost, flexibility, and suitability for large-area processing.[1] The power conversion efficiency (PCE) of PSCs based on single-layer, polymer−fullerene bulk-heterojunction solar cells has recently reached over 10%.[2−4] The two electrodes, anode, and cathode have a considerable effect on the performance of the PSCs. One of the electrodes is required to have high transparency for light transmission and absorption by the active layer. Among the various transparent electrodes, indium tin oxide (ITO) electrodes are most commonly used for PSCs.[5−8] The other electrode is required to have high reflectivity so that light can be reflected and absorbed for a second time. Metals such as Al and Ag are usually used to form this electrode.[7,8] Moreover, both electrodes should have proper work functions to match the energy levels of the charge carriers for efficient extraction of the electrons and holes. This enables good ohmic contacts and a maximum built-in potential. However, these electrodes exhibit certain drawbacks that must be addressed before further development of low-cost, efficient, and stable PSCs.

Commonly used ITO is not suitable for PSCs because of its brittleness, high-temperature processing, and high cost. Several reports have suggested alternatives to ITO, such as conducting polymers,[9,10] carbon nanotubes,[11−13] graphene,[14−16] metallic nanowires,[17−20] and metallic grids.[21,22] However, many of these alternative materials exhibit drawbacks such as large sheet resistance[13,14] or high surface roughness,[17,18,23] which reduce the fill factor (FF) and PCE of the PSC devices. Further, the work functions of these electrodes do not match with the active layers, and hence, insertion of additional interfacial materials is required for transporting and extracting electrons and holes efficiently. For the anode, poly(3,4-ethylene dioxythiophene)−polystyrene sulfonic acid (PEDOT:PSS) is the commonly used anode buffer layer in PSCs, but its hygroscopic and acidic nature has a strong impact on the stability of the PSCs, resulting in considerable performance degradation over time.[24,25] Stable metal oxides, such as MoO_3,[26] WO_3,[27] NiO,[28] and V_2O_5,[26,29] have recently been reported as alternatives to PEDOT:PSS at the anode for hole collecting. For the cathode, ZnO[24] and TiOx[30] are commonly used as cathode buffer layers in PSCs. Devices based on these oxide interface layers require annealing treatment and are affected by

Received: May 24, 2015
Accepted: September 1, 2015
Published: September 1, 2015

DOI: 10.1021/acsami.5b04509
ACS Appl. Mater. Interfaces 2015, 7, 19960−19965

a "light-soaking" problem.[31,32] They exhibit an anomalous current density and voltage (J–V) curve with an S-shape, resulting in an extremely low FF. However, as the light irradiation is prolonged, the S-shape curve disappears and the device parameters regain their expected values. Therefore, there is a pressing need for an ITO-free transparent cathode with good optoelectrical properties and low work function, as well as low cost and low-temperature processing.

The theory of induced transmission indicates that the transmittance of a metal film depends not only on its own optical constants but also on the admittances of the surrounding structures.[33] According to this theory, the transmittance can be enhanced through suitable design of an antireflection coating (dielectric layer) on either side of the metal film. Recently, transparent electrodes with dielectric–metal–dielectric (DMD) structures have attracted considerable interest because of their good optical and electrical properties.[19,34−37] The optical and electrical properties and the work function of the DMD electrodes can be controlled through selection of the dielectric and metal materials.[38−42] In this paper, a novel transparent cathode with a tin oxide (SnO_X)/Ag/SnO_X/bismuth oxide (Bi_2O_3) (SASB) structure is proposed. For the first time, Bi_2O_3 is employed as a modified layer in the DMD structure, which lowers the work function of the SAS cathode. The SASB transparent cathode exhibits excellent electrical and optical properties and a suitable work function matched with the lowest unoccupied molecular orbital (LUMO) level of the acceptor. Thus, the device performance is comparable to that of devices based on interfacial modified ITO electrodes.

RESULTS AND DISCUSSION

For transparent DMD electrodes, the electrical properties mainly depend on the middle metal layer, and the transmittance can be enhanced by adjusting the thicknesses of the two dielectric layers. In general, to realize a highly conductive film, the metal layer should be at least 10 nm thick, which can provide a continuous conducting path.[43] Therefore, in this work, an 11-nm-thick Ag layer was introduced as the metal layer to ensure low sheet resistance. The optical transmittance of the SAS transparent electrode was optimized by changing the thicknesses of the two SnO_X layers. A maximum average transmittance of 78.37% was achieved using two 30-nm-thick SnO_X layers as the two dielectric layers (Supporting Information Figure S1). The reference transmittance spectra of Ag and SnO_X/Ag (Supporting Information Figure S2) further confirmed that the transmittance of the Ag film could be increased by optimizing the thicknesses of the two SnO_X dielectric layers. Moreover, the electrical characteristics of the SAS electrode with different thicknesses of SnO_X layers are investigated by Hall measurements (Supporting Information Figure S3). The SAS electrode exhibited a sheet resistance of 9.0 $\Omega \cdot sq^{-1}$, which is lower than that of most commercial ITO electrodes.[44] According to previous studies, SnO_X has a work function of ~4.7 eV,[45] which does not match with the LUMO level of the acceptor in PSCs. Therefore, to meet the requirement that PSC cathodes have a low work function, a less well-known metal oxide Bi_2O_3 with low work function[46] was introduced in the SAS structure to form a SASB structure transparent electrode. This electrode exhibits a highest occupied molecular orbital (HOMO) level of 5.25 eV (Supporting Information Figure S4) and a band gap of 3.27 eV (Supporting Information Figure S5). Figure 1 shows the

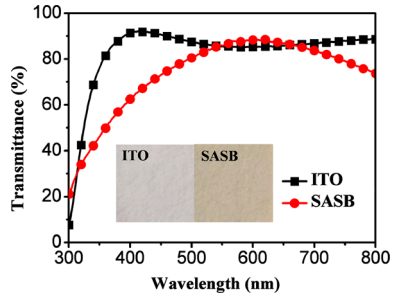

Figure 1. Transmittance spectra of ITO and SASB electrodes. Photographs of the ITO and SASB electrodes are shown in the insets.

transmittance spectra of SASB and ITO electrodes. The Bi_2O_3 layer is only several nanometers thick and, hence, has little effect on the transmittance and morphology of the electrode (Supporting Information Figures S6 and S7). Thus, the SASB electrode exhibits a maximum transmittance of 88%, similar to that of the SAS electrode. The average transmittance of the SASB electrode over the wavelength range of 400–700 nm corresponding to the absorption of the active layer of PSCs is 81.53%, while the average transmittance of ITO in the same wavelength range is 87.37%.

The impact of Bi_2O_3 on the characteristics of the SASB electrode, including its optical and electrical properties, has been studied in detail. Figure 2 shows the electrical and optical

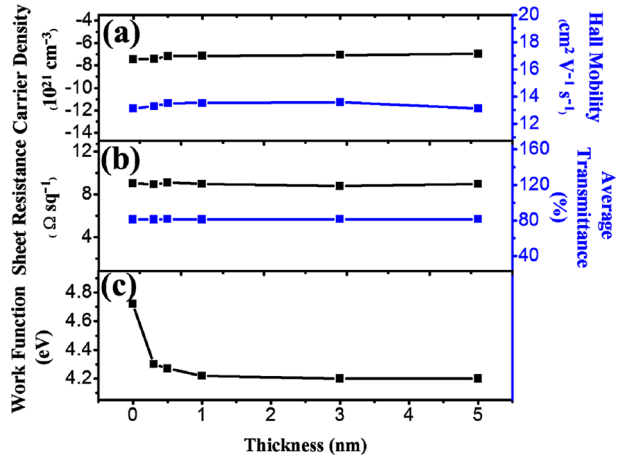

Figure 2. (a) Carrier density (black) and Hall mobility (blue), (b) sheet resistance (black) and average transmittance (blue), and (c) work function of the SASB electrodes as a function of different thicknesses of Bi_2O_3.

characteristics, including the carrier concentration, Hall mobility, sheet resistance, average transmittance, and work function of the SASB electrodes as a function of the Bi_2O_3 thicknesses of 0, 0.3, 0.5, 1, 3, and 5 nm. The carrier density, Hall mobility, sheet resistance, and average transmittance of the SASB electrode remain virtually unchanged as the thickness of Bi_2O_3 increases from 0 to 5 nm (Figure 2a and b). As shown in Figure 2c, the work function of the SAS electrode (Bi_2O_3 thickness = 0 nm) measured by a Kelvin probe system is 4.72 eV. With increasing thickness of Bi_2O_3, the work function of the SASB is reduced and reaches a relatively constant value of ~4.22 eV when the thickness of Bi_2O_3 is 1 nm.

The low work function of the SASB electrode matches well with the LUMO level of the acceptor. Figure 3 shows the

DOI: 10.1021/acsami.5b04509
ACS Appl. Mater. Interfaces 2015, 7, 19960−19965

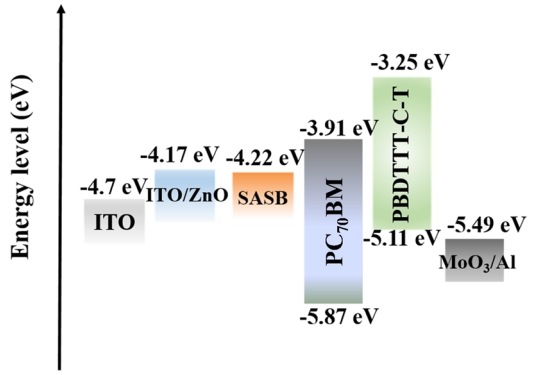

Figure 3. Energy level alignment of the materials used in PSCs.

energy level alignment of the PSC materials used in this work. For the anode of the inverted solar cell, the commonly used anode MoO_3/Al with a work function of −5.49 eV was used for extracting holes from the donor of poly[4,8-bis(2-ethylhexyl thiophene-5-yl)benzo[1,2-*b*:4,5-*b*′]dithiophene-2,6-diyl]-*alt*-[2-(2′-thylhexanoyl)thieno[3,4-*b*]thio-phen-4,6-diyl] (PBDTTT-C-T). For the cathode, ITO was used for comparison purposes. The work function of the SASB electrode (−4.22 eV) is lower than that of the ITO electrode (−4.7 eV) and is similar to that of a ZnO-modified ITO electrode (−4.17 eV), which is close to the LUMO level of the acceptor material of [6,6]-phenyl C71-butyric acid methyl ester ($PC_{70}BM$). This indicates good ohmic contact and increased built-in potential for maximizing the open-circuit voltage (V_{OC}).

To evaluate the photoelectric properties of the transparent SASB electrode, PSCs based on conjugated polymer PBDTTT-C-T and fullerene derivative $PC_{70}BM$ were prepared on SASB electrodes. Parts a and b of Figure 4 show the *J*−*V* characteristics of SASB-based PSCs with different thicknesses of Bi_2O_3 under illumination and in the dark, respectively. These parameters are summarized in detail in Table 1. SASB1−SASB5 represent SASB electrodes with Bi_2O_3 thicknesses of 0.3, 0.5, 1, 3, and 5 nm, respectively. As can be seen from Table 1, the V_{OC}, short-circuit current density (J_{SC}), FF, and PCE increased as Bi_2O_3 thickness increased from 0.3 to 0.5 nm, and they exhibited maximum values for a Bi_2O_3 thickness of 1 nm. This is attributed to the decreased work function of the SASB electrode, which enhances the built-in potential of the PSC and results in a higher V_{OC}.[47] This is also confirmed by the following equation:

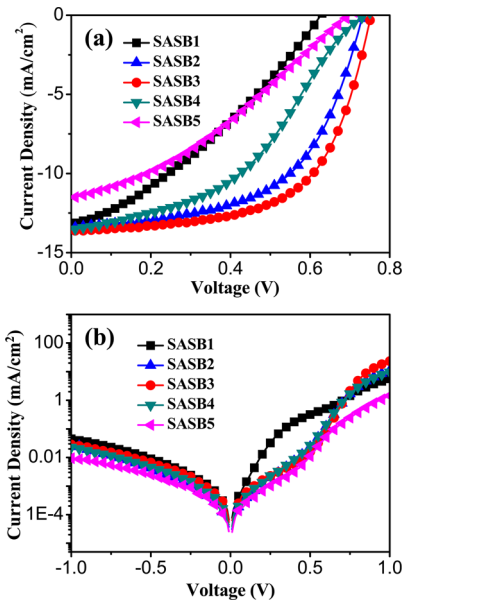

Figure 4. *J*−*V* characteristics of PSCs with different Bi_2O_3 thicknesses under (a) illumination of AM1.5 G and 100 mW/cm^2 and (b) in the dark.

$$V_{OC} = \frac{nk_BT}{q}\ln\frac{J_{SC}}{J_0} \quad (1)$$

where *T* is the temperature, k_B is the Boltzmann constant, J_0 is the reverse saturation current density, and *n* is the ideality factor. J_0 is extracted by fitting the dark *J*−*V* data[47,48] (Supporting Information Figure S8), as listed in Table 1. SASB3 shows the lowest J_0 of 1.74×10^{-7} mA·cm^{-2}, which is ∼4 orders of magnitude lower than that of the SASB1 device. Therefore, according to the above equation, the largest V_{OC} should appear in the device with 1-nm-thick Bi_2O_3. Moreover, the modified ohmic contact between the SASB electrode and the active layer results in a reduced series resistance (R_S) from 19.15 Ω·cm^2 at 0.3 nm to 5.54 Ω·cm^2 at 1 nm and an increased sheet resistance (R_{sh}) from 0.96 MΩ·cm^2 at 0.3 nm to 3.51 MΩ·cm^2 at 1 nm. However, on further increasing the Bi_2O_3 thickness, all device parameters noticeably deteriorate, indicating that the transporting and extracting of electrons are hindered by a thick Bi_2O_3 layer.[7] Therefore, an optimized PCE of 6.21%, with a V_{OC} of 0.75 V, J_{SC} of 13.66 mA·cm^{-2}, and FF of 0.61 was realized using a 1-nm-thick Bi_2O_3 layer in an SASB-based device.

To confirm the role of Bi_2O_3 in lowering the work function of the electrode, PSC devices based on different Bi_2O_3-modified ITO electrodes were studied for comparison (Supporting Information Figure S9 and Table S1). The comparison provides a similar conclusion that the device based on an ITO electrode with a 1-nm-thick Bi_2O_3 layer exhibits an optimized PCE of 6.54%, with a V_{OC} of 0.75 V, J_{SC} of 14.97 mA·cm^{-2}, and FF of 0.58. A reference device with the commonly used ITO/ZnO cathode was also fabricated, and it exhibits a PCE of 6.58% with a V_{OC} of 0.75 V, J_{SC} of 14.89 mA·cm^{-2}, and FF of 0.59. The *J*−*V* characteristics of the optimized devices based on SASB, ITO/Bi_2O_3, and ITO/ZnO electrodes are summarized in Figure 5a, and the device parameters are listed in Table 1. Owing to the lower transmittance of SASB in the short-wavelength range (Figure 1), PSCs based on SASB electrodes exhibit a smaller J_{SC} and, thus, a smaller PCE compared with devices based on ITO/Bi_2O_3 and ITO/ZnO electrodes. This result was confirmed by the external quantum efficiency (EQE) spectra (Figure 5b) and the J_{SC} values calculated from the EQE spectra (Table 1) of the devices based on different cathodes. The competitive performance of the SASB device indicates that SASB can replace ITO as transparent cathodes in optoelectronic devices.

CONCLUSION

We have developed a low-work-function, ITO-free, transparent SASB cathode, in which Bi_2O_3 was introduced to lower the work function of the transparent electrode. The SASB electrode shows excellent optical and electrical properties without annealing treatment, including a maximum transmittance of 88% and a low sheet resistance of ∼9.0 Ω·sq^{-1}, as well as a low work function of 4.22 eV, which is suitable for extraction of

DOI: 10.1021/acsami.5b04509
ACS Appl. Mater. Interfaces 2015, 7, 19960−19965

Table 1. Performance of PSCs Based on Different Substrates

device	V_{OC} [V]	J_{SC} [mA·cm^{-2}]	FF	PCE [%]	R_S [Ω·cm^2]	R_{sh} [MΩ·cm^2]	J_{EQE} [mA·cm^{-2}]	J_0 [mA·cm^{-2}]
SASB1	0.63	13.24	0.33	2.75	19.15	0.96	13.20	3.21×10^{-3}
SASB2	0.73	13.38	0.56	5.52	7.42	1.49	13.32	1.46×10^{-6}
SASB3	0.75	13.66	0.61	6.21	5.54	3.51	13.65	1.74×10^{-7}
SASB4	0.72	12.83	0.38	3.49	26.96	1.94	12.77	2.22×10^{-6}
SASB5	0.70	11.55	0.34	2.71	46.58	1.43	11.24	3.36×10^{-6}
ITO/Bi_2O_3 (1 nm)	0.75	14.97	0.58	6.54	6.06	2.21	14.96	
ITO/ZnO	0.75	14.89	0.59	6.58	6.65	1.93	14.84	

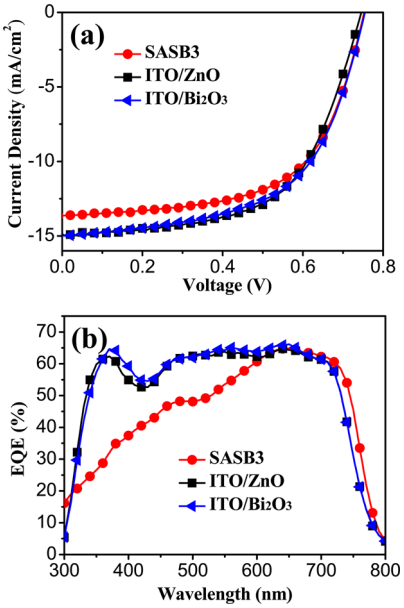

Figure 5. (a) $J-V$ characteristics and (b) EQE spectra of the PSCs based on different electrodes.

electrons from the cathode of PSCs. The effect of Bi_2O_3 thickness on the photoelectric properties of the SASB electrodes has also been investigated. The PCE of the inverted PSC based on the SASB electrode is 6.21%, which is comparable to that of ITO-based devices. This result indicates that SASB is a good alternative to ITO as transparent cathodes in optoelectronic devices.

EXPERIMENTAL METHODS

SASB Electrode Fabrication and Characterization. The SASB films were deposited on a precleaned polished glass substrate by electron beam evaporation at room temperature. The thickness of the SnO_X layers was varied between 20 and 50 nm, while the silver layer thickness was fixed at 11 nm. The evaporation rate of SnO_X and Ag was 0.3−0.4 nm·s^{-1} and 0.7−1.0 nm·s^{-1} in vacuum at pressures lower than 2.0×10^{-3} Pa. The sheet resistance was measured using the four-probe method. The carrier concentration and Hall mobility of the SASB films were determined using a HMS-3000 Hall effect measurement system with an applied magnetic field of 0.55 T. The surface work function of the SASB films was measured using a KP Technology Ambient Kelvin probe system package. The film thicknesses were calibrated using an Ambios XP-1 surface profiler. The transmittance spectra of the SASB samples were recorded using a Shimadzu UV-3101PC spectrophotometer. The atomic force microscopy (AFM) measurement was performed on a Shimadzu SPM-9700. All measurements of the optoelectrical properties were performed at room temperature.

PSC Fabrication and Characterization. SnO_X (30 nm), Ag (11 nm), SnO_X (30 nm), and Bi_2O_3 (different thicknesses) were deposited sequentially by electron beam evaporation through a shadow mask at room temperature. An active layer consisting of a blend of the low-bandgap conjugated polymer PBDTTT-C-T (Solarmer) and $PC_{70}BM$ (American Dye) was spin-coated onto the substrates from dichlorobenzene in a glovebox. A small amount (3% in volume ratio) of a high-boiling-point additive 1,8-diiodooctane (DIO, Sigma-Aldrich) was used in order to optimize the morphology. Finally, MoO_3 (8 nm) and Al (100 nm) were thermally deposited at a pressure of ~4×10^{-4} Pa. The $J-V$ characteristics of the PSCs were measured using a computer-controlled Keithley 2611 source meter under AM 1.5G illumination from a calibrated solar simulator with an irradiation intensity of 100 mW·cm^{-2}. EQE measurements were performed with a lock-in amplifier at a chopping frequency of 20 Hz under illumination by monochromatic light from a xenon lamp.

ASSOCIATED CONTENT

Supporting Information

The Supporting Information is available free of charge on the ACS Publications website at DOI: 10.1021/acsami.5b04509.

Optical and electrical properties, AFM, UPS, $J-V$, and EQE (PDF)

AUTHOR INFORMATION

Corresponding Authors

*E-mail: liuxy@ciomp.ac.cn.

*E-mail: guoxy@ciomp.ac.cn.

Notes

The authors declare no competing financial interest.

ACKNOWLEDGMENTS

This work is supported by the CAS Innovation Program, the National Natural Science Foundation of China nos. 61106057 and 6140031454, the Jilin Province Science and Technology Research Project nos. 20140520119JH and 20150101039JC, and project supported by State Key Laboratory of Luminescence and Applications.

REFERENCES

(1) Mazzio, K. A.; Luscombe, C. K. The Future of Organic Photovoltaics. *Chem. Soc. Rev.* **2015**, *44*, 78−90.

(2) He, Z.; Xiao, B.; Liu, F.; Wu, H.; Yang, Y.; Xiao, S.; Wang, C.; Russell, T. P.; Cao, Y. Single-Junction Polymer Solar Cells with High Efficiency and Photovoltage. *Nat. Photonics* **2015**, *9*, 174−179.

(3) Liu, Y.; Zhao, J.; Li, Z.; Mu, C.; Ma, W.; Hu, H.; Jiang, K.; Lin, H.; Ade, H.; Yan, H. Aggregation and Morphology Control Enables Multiple Cases of High-Efficiency Polymer Solar Cells. *Nat. Commun.* **2014**, *5*, 5293.

(4) Liao, S.-H.; Jhuo, H.-J.; Yeh, P.-N.; Cheng, Y.-S.; Li, Y.-L.; Lee, Y.-H.; Sharma, S.; Chen, S.-A. Single Junction Inverted Polymer Solar Cell Reaching Power Conversion Efficiency 10.31% by Employing Dual-Doped Zinc Oxide Nano-Film as Cathode Interlayer. *Sci. Rep.* **2014**, *4*, 6813.

(5) Choi, J. K.; Jin, M. L.; An, C. J.; Kim, D. W.; Jung, H. T. High-Performance of PEDOT/PSS Free Organic Solar Cells on an Air-

DOI: 10.1021/acsami.5b04509
ACS Appl. Mater. Interfaces 2015, 7, 19960−19965

Plasma-Treated ITO Substrate. *ACS Appl. Mater. Interfaces* **2014**, *6*, 11047−11053.
(6) Lei, H. W.; Qin, P. L.; Ke, W. J.; Guo, Y. X.; Dai, X.; Chen, Z.; Wang, H. N.; Li, B. R.; Zheng, Q.; Fang, G. J. Performance Enhancement of Polymer Solar Cells with High Work Function CuS Modified ITO as Anodes. *Org. Electron.* **2015**, *22*, 173−179.
(7) Qi, B.; Zhang, Z.-G.; Wang, J. Uncovering the Role of Cathode Buffer Layer in Organic Solar Cells. *Sci. Rep.* **2015**, *5*, 7803.
(8) Po, R.; Carbonera, C.; Bernardi, A.; Camaioni, N. The Role of Buffer Layers in Polymer Solar Cells. *Energy Environ. Sci.* **2011**, *4*, 285−310.
(9) Ha, Y. H.; Nikolov, N.; Pollack, S. K.; Mastrangelo, J.; Martin, B. D.; Shashidhar, R. Towards a Transparent, Highly Conductive Poly(3,4-ethylenedioxythiophene). *Adv. Funct. Mater.* **2004**, *14*, 615−622.
(10) Vosgueritchian, M.; Lipomi, D. J.; Bao, Z. Highly Conductive and Transparent PEDOT:PSS Films with a Fluorosurfactant for Stretchable and Flexible Transparent Electrodes. *Adv. Funct. Mater.* **2012**, *22*, 421−428.
(11) Tenent, R. C.; Barnes, T. M.; Bergeson, J. D.; Ferguson, A. J.; To, B.; Gedvilas, L. M.; Heben, M. J.; Blackburn, J. L. Ultrasmooth, Large-Area, High-Uniformity, Conductive Transparent Single-Walled-Carbon-Nanotube Films for Photovoltaics Produced by Ultrasonic Spraying. *Adv. Mater.* **2009**, *21*, 3210−3216.
(12) Barnes, T. M.; Reese, M. O.; Bergeson, J. D.; Larsen, B. A.; Blackburn, J. L.; Beard, M. C.; Bult, J.; van de Lagemaat, J. Comparing the Fundamental Physics and Device Performance of Transparent, Conductive Nanostructured Networks with Conventional Transparent Conducting Oxides. *Adv. Energy Mater.* **2012**, *2*, 353−360.
(13) Salvatierra, R. V.; Cava, C. E.; Roman, L. S.; Zarbin, A. J. G. ITO-Free and Flexible Organic Photovoltaic Device Based on High Transparent and Conductive Polyaniline/Carbon Nanotube Thin Films. *Adv. Funct. Mater.* **2013**, *23*, 1490−1499.
(14) De, S.; Coleman, J. N. Are There Fundamental Limitations on the Sheet Resistance and Transmittance of Thin Graphene Films. *ACS Nano* **2010**, *4*, 2713−2720.
(15) Yin, Z.; Sun, S.; Salim, T.; Wu, S.; Huang, X.; He, Q.; Lam, Y. M.; Zhang, H. Organic Photovoltaic Devices Using Highly Flexible Reduced Graphene Oxide Films as Transparent Electrodes. *ACS Nano* **2010**, *4*, 5263−5268.
(16) Chen, X.; Jia, B.; Zhang, Y.; Gu, M. Exceeding the Limit of Plasmonic Light Trapping in Textured Screen-Printed Solar Cells Using Al Nanoparticles and Wrinkle-Like Graphene Sheets. *Light: Sci. Appl.* **2013**, *2*, e92.
(17) De, S.; Higgins, T. M.; Lyons, P. E.; Doherty, E. M.; Nirmalraj, P. N.; Blau, W. J.; Boland, J. J.; Coleman, J. N. Silver Nanowire Networks as Flexible, Transparent, Conducting Films: Extremely High DC to Optical Conductivity Ratios. *ACS Nano* **2009**, *3*, 1767−1774.
(18) Rathmell, A. R.; Bergin, S. M.; Hua, Y.-L.; Li, Z.-Y.; Wiley, B. J. The Growth Mechanism of Copper Nanowires and Their Properties in Flexible, Transparent Conducting Films. *Adv. Mater.* **2010**, *22*, 3558−3563.
(19) Wilken, S.; Wilkens, V.; Scheunemann, D.; Nowak, R.-E.; von Maydell, K.; Parisi, J.; Borchert, H. Semitransparent Polymer-Based Solar Cells with Aluminum-Doped Zinc Oxide Electrodes. *ACS Appl. Mater. Interfaces* **2015**, *7*, 287−300.
(20) Liu, J. W.; Wang, J. L.; Wang, Z. H.; Huang, W. R.; Yu, S. H. Manipulating Nanowire Assembly for Flexible Transparent Electrodes. *Angew. Chem.* **2014**, *126*, 13695−13700.
(21) Zou, J.; Yip, H.-L.; Hau, S. K.; Jen, A. K.-Y. Metal Grid/Conducting Polymer Hybrid Transparent Electrode for Inverted Polymer Solar Cells. *Appl. Phys. Lett.* **2010**, *96*, 203301.
(22) Wu, H.; Menon, M.; Gates, E.; Balasubramanian, A.; Bettinger, C. J. Reconfigurable Topography for Rapid Solution Processing of Transparent Conductors. *Adv. Mater.* **2014**, *26*, 706−711.
(23) Lee, J.-Y.; Connor, S. T.; Cui, Y.; Peumans, P. Solution-Processed Metal Nanowire Mesh Transparent Electrodes. *Nano Lett.* **2008**, *8*, 689−692.
(24) Sun, Y.; Seo, J. H.; Takacs, C. J.; Seifter, J.; Heeger, A. J. Inverted Polymer Solar Cells Integrated with a Low-Temperature-Annealed Sol-Gel-Derived ZnO Film as an Electron Transport Layer. *Adv. Mater.* **2011**, *23*, 1679−1683.
(25) Garcia, A.; Welch, G. C.; Ratcliff, E. L.; Ginley, D. S.; Bazan, G. C.; Olson, D. C. Improvement of Interfacial Contacts for New Small-Molecule Bulk-Heterojunction Organic Photovoltaics. *Adv. Mater.* **2012**, *24*, 5368−5373.
(26) Li, X.; Xie, F.; Zhang, S.; Hou, J.; Choy, W. C. MoOx and V_2Ox as Hole and Electron Transport Layers Through Functionalized Intercalation in Normal and Inverted Organic Optoelectronic Devices. *Light: Sci. Appl.* **2015**, *4*, e273.
(27) Han, S.; Shin, W. S.; Seo, M.; Gupta, D.; Moon, S.-J.; Yoo, S. Improving Performance of Organic Solar Cells Using Amorphous Tungsten Oxides as an Interfacial Buffer Layer on Transparent Anodes. *Org. Electron.* **2009**, *10*, 791−797.
(28) Zhai, Z.; Huang, X.; Xu, M.; Yuan, J.; Peng, J.; Ma, W. Greatly Reduced Processing Temperature for a Solution-Processed NiOx Buffer Layer in Polymer Solar Cells. *Adv. Energy Mater.* **2013**, *3*, 1614−1622.
(29) Bao, X.; Zhu, Q.; Wang, T.; Guo, J.; Yang, C.; Yu, D.; Wang, N.; Chen, W.; Yang, R. Simple O_2 Plasma-Processed V_2O_5 as an Anode Buffer Layer for High-Performance Polymer Solar Cells. *ACS Appl. Mater. Interfaces* **2015**, *7*, 7613−7618.
(30) Yoo, B.; Kim, K.; Lee, S. H.; Kim, W. M.; Park, N.-G. ITO/ATO/TiO_2 Triple-Layered Transparent Conducting Substrates for Dye-Sensitized Solar Cells. *Sol. Energy Mater. Sol. Cells* **2008**, *92*, 873−877.
(31) Shao, S.; Liu, J.; Zhang, B.; Xie, Z.; Wang, L. Enhanced Stability of Zinc Oxide-Based Hybrid Polymer Solar Cells by Manipulating Ultraviolet Light Distribution in the Active Layer. *Appl. Phys. Lett.* **2011**, *98*, 203304.
(32) Kim, J.; Kim, G.; Choi, Y.; Lee, J.; Park, S. H.; Lee, K. Light-Soaking Issue In Polymer Solar Cells: Photoinduced Energy Level Alignment at the Sol-Gel Processed Metal Oxide and Indium Tin Oxide Interface. *J. Appl. Phys.* **2012**, *111*, 114511.
(33) Berning, P. H.; Turner, A. F. Induced Transmission in Aborbing Films Applied to Band Pass Filter Design. *J. Opt. Soc. Am.* **1957**, *47*, 230−239.
(34) Xu, W.-F.; Chin, C.-C.; Hung, D.-W.; Wei, P.-K. Transparent Electrode for Organic Solar Cells Using Multilayer Structures with Nanoporous Silver Film. *Sol. Energy Mater. Sol. Cells* **2013**, *118*, 81−89.
(35) Yun, J.; Wang, W.; Bae, T. S.; Park, Y. H.; Kang, Y. C.; Kim, D. H.; Lee, S.; Lee, G. H.; Song, M.; Kang, J. W. Preparation of Flexible Organic Solar Cells with Highly Conductive and Transparent Metal-Oxide Multilayer Electrodes Based on Silver Oxide. *ACS Appl. Mater. Interfaces* **2013**, *5*, 9933−9941.
(36) Yambem, S. D.; Ullah, M.; Tandy, K.; Burn, P. L.; Namdas, E. B. ITO-Free Top Emitting Organic Light Emitting Diodes with Enhanced Light Out-Coupling. *Laser Photonics Rev.* **2014**, *8*, 165−171.
(37) Wang, W.; Song, M.; Bae, T.-S.; Park, Y. H.; Kang, Y.-C.; Lee, S.-G.; Kim, S.-Y.; Kim, D. H.; Lee, S.; Min, G.; Lee, G.-H.; Kang, J.-W.; Yun, J. Transparent Ultrathin Oxygen-Doped Silver Electrodes for Flexible Organic Solar Cells. *Adv. Funct. Mater.* **2014**, *24*, 1551−1561.
(38) Park, Y.-S.; Park, H.-K.; Jeong, J.-A.; Kim, H.-K.; Choi, K.-H.; Na, S.-I.; Kim, D.-Y. Comparative Investigation of Transparent ITO/Ag/ITO and ITO/Cu/ITO Electrodes Grown by Dual-Target DC Sputtering for Organic Photovoltaics. *J. Electrochem. Soc.* **2009**, *156*, H588−H594.
(39) Winkler, T.; Schmidt, H.; Flügge, H.; Nikolayzik, F.; Baumann, I.; Schmale, S.; Weimann, T.; Hinze, P.; Johannes, H.-H.; Rabe, T.; Hamwi, S.; Riedl, T.; Kowalsky, W. Efficient Large Area Semi-transparent Organic Solar Cells Based on Highly Transparent and Conductive ZTO/Ag/ZTO Multilayer Top Electrodes. *Org. Electron.* **2011**, *12*, 1612−1618.
(40) Choi, Y.-Y.; Choi, K.-H.; Lee, H.; Lee, H.; Kang, J.-W.; Kim, H.-K. Nano-Sized Ag-Inserted Amorphous $ZnSnO_3$ Multilayer Electrodes

DOI: 10.1021/acsami.5b04509
ACS Appl. Mater. Interfaces 2015, 7, 19960−19965

for Cost-Efficient Inverted Organic Solar Cells. *Sol. Energy Mater. Sol. Cells* **2011**, *95*, 1615−1623.
(41) Xue, Z.; Liu, X.; Zhang, N.; Chen, H.; Zheng, X.; Wang, H.; Guo, X. High-Performance NiO/Ag/NiO Transparent Electrodes for Flexible Organic Photovoltaic Cells. *ACS Appl. Mater. Interfaces* **2014**, *6*, 16403−16408.
(42) Guo, X.; Lin, J.; Chen, H.; Zhang, X.; Fan, Y.; Luo, J.; Liu, X. Ultrathin and Efficient Flexible Polymer Photovoltaic Cells Based on Stable Indium-Free Multilayer Transparent Electrodes. *J. Mater. Chem.* **2012**, *22*, 17176−17182.
(43) Cattin, L.; Bernède, J. C.; Morsli, M. Toward Indium-Free Optoelectronic Devices: Dielectric/Metal/Dielectric Alternative Transparent Conductive Electrode in Organic Photovoltaic Cells. *Phys. Status Solidi A* **2013**, *210*, 1047−1061.
(44) Ellmer, K. Past Achievements and Future Challenges in the Development of Optically Transparent Electrodes. *Nat. Photonics* **2012**, *6*, 809−817.
(45) Yang, J.-D.; Cho, S.-H.; Hong, T.-W.; Son, D. I.; Park, D.-H.; Yoo, K.-H.; Choi, W.-K. Organic Photovoltaic Cells Fabricated on a SnOx/Ag/SnOx Multilayer Transparent Conducting Electrode. *Thin Solid Films* **2012**, *520*, 6215−6220.
(46) Morasch, J.; Li, S.; Brötz, J.; Jaegermann, W.; Klein, A. Reactively Magnetron Sputtered Bi_2O_3 Thin Films: Analysis of Structure, Optoelectronic, Interface, and Photovoltaic Properties. *Phys. Status Solidi A* **2014**, *211*, 93−100.
(47) Qi, B.; Wang, J. Open-Circuit Voltage in Organic Solar Cells. *J. Mater. Chem.* **2012**, *22*, 24315−24325.
(48) Vandewal, K.; Tvingstedt, K.; Gadisa, A.; Inganas, O.; Manca, J. V. On the Origin of the Open-Circuit Voltage of Polymer-Fullerene Solar Cells. *Nat. Mater.* **2009**, *8*, 904−909.

DOI: 10.1021/acsami.5b04509
ACS Appl. Mater. Interfaces 2015, 7, 19960−19965